SAND2018-14184C

Study of Sensitivity vs. Excitation Time of LED Excited Thermographic Phosphor

Wendy Flores-Brito[1]
Sandia National Laboratories, Albuquerque, New Mexico, 87123, United States

Eric Westphal.[2]
Purdue University, West Lafayette, Indiana, 47907, United States

Bethany R. Wilburn[3]
The University of Texas at El Paso, El Paso, Texas, 79968, United States

and
Kathryn N. G. Hoffmeister[4]
Sandia National Laboratories, Albuquerque, New Mexico, 87123, United States

The excitation of $Mg_3F_2GeO_4$:Mn thermographic phosphors using a UV LED centered at 365 nm is explored. Two different LED drivers, one available commercially and one built at Sandia National Laboratories (SNL), were used and assessed for their viability for phosphor thermometry utilizing LED excitation and intensified, high-speed, CMOS camera data collection. The SNL-driven LED was then utilized as an excitation source for $Mg_3F_2GeO_4$:Mn-phosphor calibration and demonstration experiments measuring the temperature of a silicon carbide heating rod using the time-decay method. The results presented here serve as a step toward determining the application space, wherein SNL driven LED excitation would be preferable over the use of laser systems for thermographic phosphor measurements.

I. Nomenclature

CMOS = complementary metal-oxide semiconductor
GOS = gadolinium oxysulfide
LED = light emitting diode
SNL = Sandia National Laboratories
YAG = yttrium aluminum garnet

II. Introduction

The importance of monitoring temperature within transient reacting environments, such as those experienced by burning materials, has driven the development of advanced diagnostic techniques. More conventional temperature-sensing techniques are often ill-suited for measuring fast-changing surfaces - whether due to sensitivity to the changing surface emissivity (in the case of bolometers), graybody assumptions (in the case of pyrometers), or potential interactions with the surfaces (in the case of thermocouples). Thermographic phosphor technology has been developed to allow remote temperature sensing with high spatial and temporal resolutions, while remaining robust in harsh reacting environments. Take intumescent paints for example. When exposed to heat the paint foams up 40-fold to form a thick and porous charred layer, which protects the coated material against heat transfer. The dense char layer not only acts as a thermal barrier but also helps both in reducing the propagation of volatiles to the flame and in shielding the coated material from oxygen transport, thus reducing the rate of flame spread. The surface temperature is an important parameter in the heat balance equation concerned with the paint and the surrounding environment, i.e.

[1] Intern Year Round – R&D Grad, Fire Science and Technology, and AIAA Student Member.
[2] Research Assistant, Department of Aerospace Engineering.
[3] Research Assistant, Department of Mechanical Engineering.
[4] R&D S&E Mechanical Engineer, Fire Science and Technology, and AIAA Member.

it is crucial for the determination of heat transfer inwards and outwards through the coating. Since the coating is very fragile, no optical or physical probe technique had succeeded previously in measuring the coating temperature [1]. However, surface temperature of an intumescent coating has been investigated using thermographic phosphors [2-6].

Typical thermographic phosphors are inorganic crystals (often oxides such as GOS or YAG), doped with luminescent centers (such as rare earth ions). It is difficult to generalize due to the large variety of phosphors available, but many phosphors, such as YAG:Dy and $Mg_3F_2GeO_4$:Mn, are ideal for combustion and fire research due to their high melting temperatures and relative insensitivity to environmental changes, such as pressure and chemical composition.

When exposed to a UV light source, electrons found in the luminescent centers of the phosphor particles are excited to higher energy levels. As the electrons relax to their equilibrium states, photons of light are given off. For inorganic phosphors, this process is called fluorescence (for decay times from less than 10^{-10} to 10^{-7}) or phosphorescence (for decay times from 10^{-5} to greater than 10^{3}) [7]. Thermographic phosphors are a subset of phosphors whose induced emissions are temperature-dependent, allowing for use in thermometry in one of two ways. The first is the lifetime of the induced emission, which typically decreases with increasing temperature [8]. Measuring the lifetime of the phosphorescence from the thermographic phosphors can therefore be used to track temperature.

The second type of phosphor thermometry is derived from changes in the spectrum of the induced emission. The spectra produced by various thermographic phosphors will shift as the equilibrium Boltzmann distribution of electrons in the phosphor changes with temperature, causing a shift in the relative numbers of electrons transitioning between a given set of energy levels. Two spectral bands are selected for a given thermographic phosphor, one with luminescent strength that stays constant with temperature, and one with intensity that either increases or decreases when the phosphor is heated. A ratio of the intensity of the two spectral bands is taken in order to minimize the effects of phosphor concentration, signal absorption, excitation source intensity, and other potential sources of error. Both of these approaches to phosphor thermometry have been applied for temperature sensing within various experimental setups, including mock gas turbine engines [9-13,15] and diesel engines [14].

Typically, laser systems are used for excitation of the thermographic phosphors, as these provide sufficient power for the phosphor signal to be easily imaged. Nd:YAG lasers are often used for excitation of thermographic phosphors, as the third and fourth harmonic of this laser (355 nm and 266 nm, respectively) can excite many thermographic phosphors. In addition, studies have also shown that excitation via light emitting diode (LED) can also yield usable signals for phosphor thermometry [1,15–18]. These studies used LEDs within the blue-UV region (100nm-495nm), allowing for excitation in a similar manner to the third and fourth harmonics of an Nd:YAG laser. Phosphorescence was collected in references [1,15-18] using a photomultiplier, as the gain provided by this imaging device is required for observing the lower emission yield produced by LED excitation when compared to laser excitation. Though the lower power of LEDs should be taken into consideration when performing phosphor thermometry, LEDs still provide many advantages over lasers for excitation, such as reduced cost, reduced complexity, and the ability to be deployed in field applications where space may be limited.

In order to increase the LED energy, longer pulse widths must be used. When using the lifetime method, it is important not to exceed the measured time constant., otherwise, it is necessary to deconvolve the LED pulse shape from that of the collected time-resolved emission data [1]. When utilizing camera technology, it is much more difficult to deconvolve this, as the time steps in data measurements are much larger, often on the order of the pulse width of the LED excitation. This, in addition to the need for time-resolved data, severely limits the LED pulse widths available for temperature measurements in fires.

III. Experimental Methods

A. Sample Preparation

The $Mg_3F_2GeO_4$:Mn (EQD25/N-U1) thermographic phosphors are available commercially from Phosphor Technology Ltd. Samples were prepared by mixing the particles with methanol and pouring the mixture onto the surface of a stainless-steel substrate or brushing it onto the surface of a silicon carbide rod. The methanol was allowed to evaporate, leaving the phosphor particles coated to the surface. Once samples were prepared, they were positioned within one of the experimental setups described below for LED excitation.

B. LED Driver Pulse Characterization Experimental Setup

A commercial, Lightspeed Technology, HPLS-36DD18B LED driver and the custom-built SNL driver (Model 614-10) [11,12] were characterized and compared. In all experiments performed in this study, a flat lens LED star array (LED Engine, LZ4-44UV00-0000) centered at 365 nm was used to excite the thermographic phosphors; the same model of LED is used with both types drivers during characterization. Fig. 1 represents the experimental setup

used to compare both LED driver's performances. A Stanford Research Systems (DG645) delay generator was used to control the 10 Hz pulse signal sent to each driver, to provide consistency in the comparison. The driver is placed in front of one of the ports of the integrating sphere, where the light is collected and transported with an Ocean Optics fiber optic cable to the photodiode (PDA10A). The output signal from the photodiode was then recorded using a Keysight Technologies InfiniiVision 200 X-series oscilloscope.

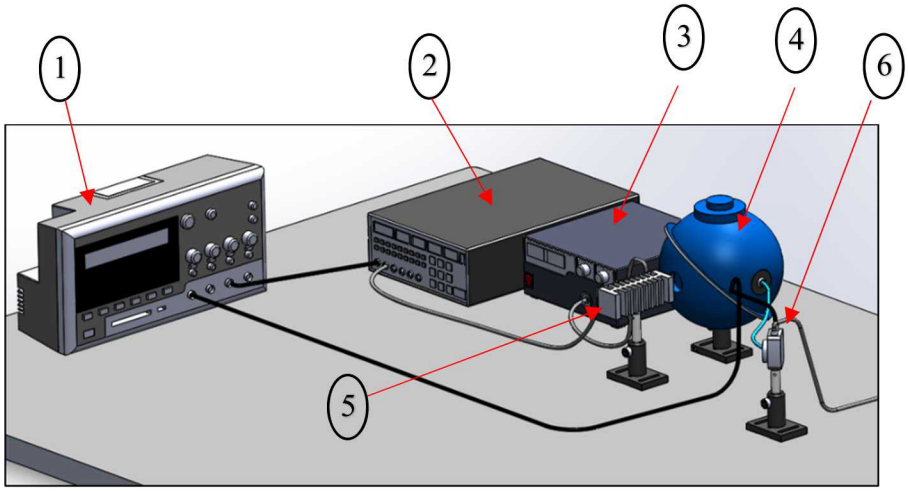

ID Number	Description
1	Oscilloscope
2	Delay Generator
3	DC Power Supply
4	Integrating Sphere
5	LED Driver
6	Photodiode

Fig. 1 Experimental setup used for LED pulse characterization experiments.

C. Phosphor Calibration Experimental Setup

The $Mg_3F_2GeO_4$:Mn phosphors were calibrated for their temperature response via LED excitation within a custom-built, high temperature furnace (Mellen). This furnace has a circular window on one side to allow the LED light to illuminate the sample, and a rectangular window on its door for imaging the phosphorescence from the phosphor sample. These windows are exactly perpendicular to one another. The SNL LED driver was used for excitation in these experiments. Two plano-convex lenses (Lattice Electro Optics) were used to focus the LED light onto a sample within the furnace in order to increase the LED intensity on the sample surface. The sample used in these experiments was prepared via the methanol evaporation method described previously. A Phantom high-speed camera (Vision Research, VEO710L) was coupled with an image intensifier (LaVision) for imaging the induced emission from the phosphor sample. A 50mm, f1.4 Nikon lens equipped with a bandpass filter centered at 660 nm (FWHM 10 nm, ASAHI) was used to capture the time-dependent phosphor signal. Similar spectral bands have been imaged with this phosphor in literature [1,8,14,21-25].

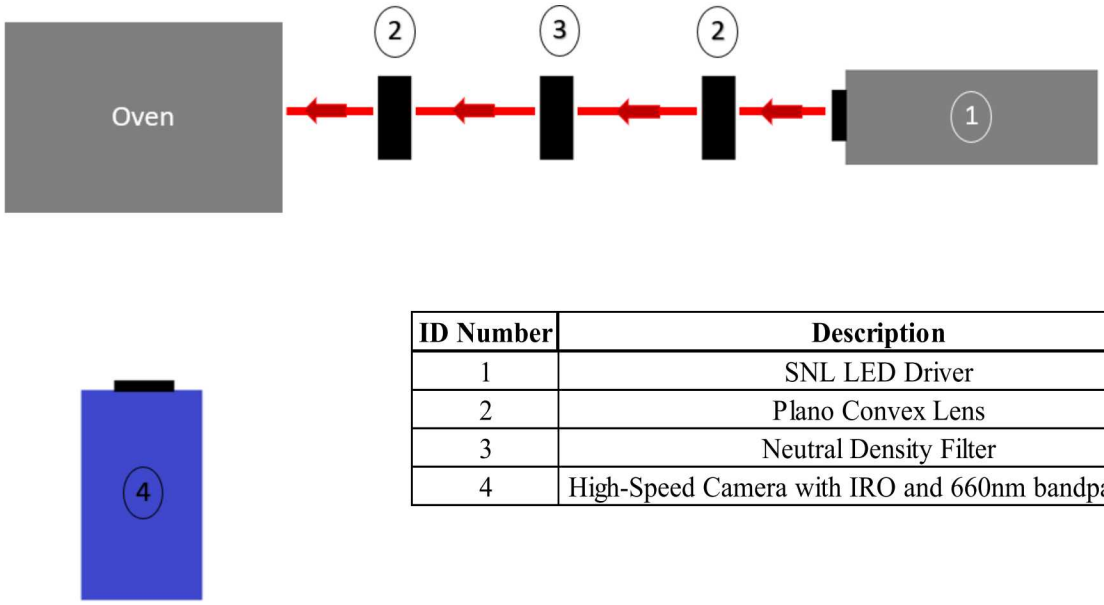

ID Number	Description
1	SNL LED Driver
2	Plano Convex Lens
3	Neutral Density Filter
4	High-Speed Camera with IRO and 660nm bandpass filter

Fig. 2 Phosphor calibration experimental setup sketch.

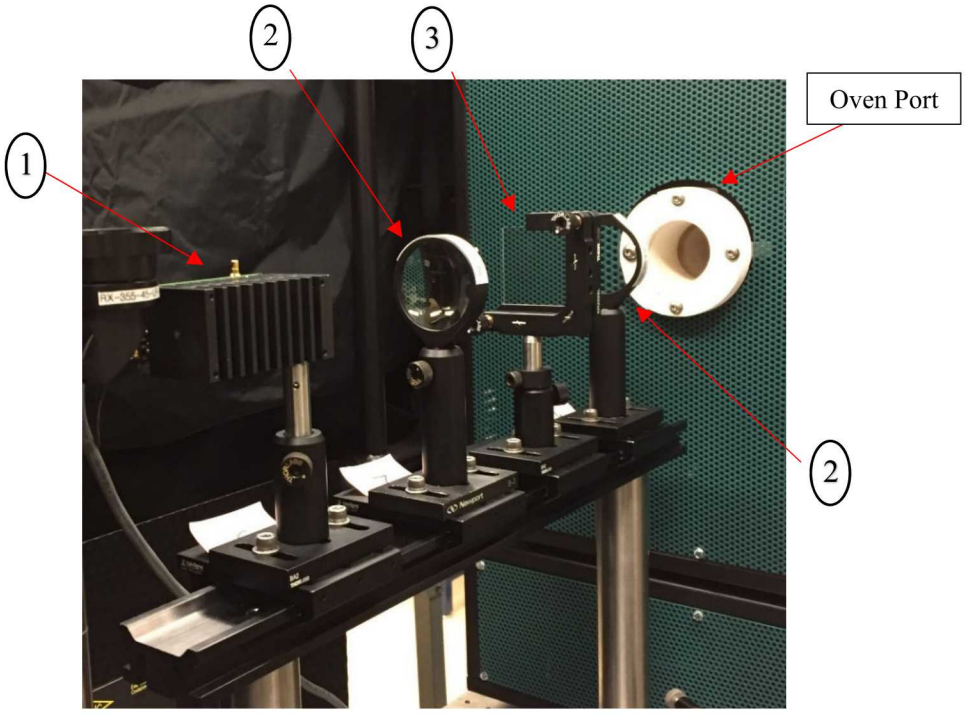

Fig. 3 SNL LED driver setup focusing into the calibration oven (ID numbers are the same as in the sketch in Fig. 2).

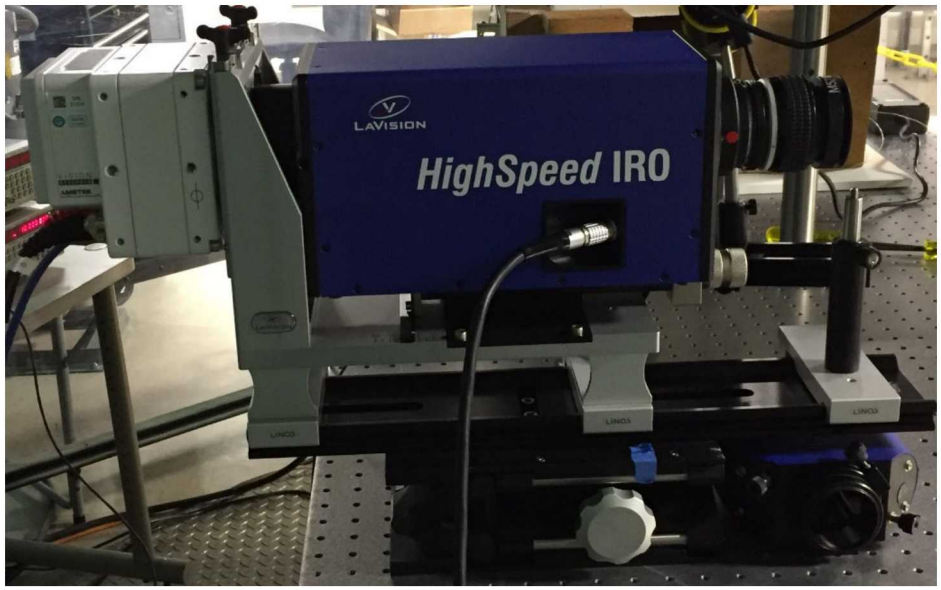

Fig. 4 LaVision High-Speed Phantom camera with a High-Speed IRO (intensifier) and a 660nm filter lens.

D. Silicon Carbide Rod Temperature Measurement Demonstration

The time-decay temperature measurements utilizing $Mg_3F_2GeO_4$:Mn phosphor were demonstrated by measuring the temperature of a silicon carbide rod in a box as it was cycled on and off. A handheld Fluke meter was used to control the applied amperage (4 mA) to the box heater consisting of four silicon carbide rods in series. An area of phosphor was painted on the second rod from the top (seen as a red patch in Fig. 5) using the method described in Section A. The same camera setup described in Section C was used to acquire data at a rate of 250 kHz.

Fig. 5 Picture of the box heater used for the demonstration experiments (left) and its power control (right).

IV. Results and Discussion

A. LED Driver Pulse Characterization

As a first step taken in characterizing the light pulses supplied by each driver, a series of pulses were sent to each driver with varying pulse durations (1, 2, 3, 4, and 5 μs). The voltage sent to the SNL driver was set to 24 V in order to give a direct comparison of the power output of each driver. The light pulses measured using the photodiode and oscilloscope. Averages over five pulses are plotted in Fig. 6 below. For simplicity, the traces from the SNL-driven pulses are shown in blue, while the commercially-driven pulses are shown in red. For the 1-3 μs pulses, the SNL-driven and commercially-driven pulses have similar shapes and rise times. However, the SNL driver produces more powerful light pulses, reaching higher voltages than those created by the commercial driver. The ratio of pulse energies (calculated by integrating the measured powers) can be found in Table 1. At longer pulse widths, it can clearly be seen that the commercial driver does not illuminate the LED for the full 4-5 μs, as the signal from this driver begins to fall slightly after 3 μs have elapsed. This is due to internal circuitry meant to limit the pulse widths to ≤1 μs. While meant as a safety feature, this circuitry severely limits the ability to vary LED pulse energy via pulse width using the commercial driver. Since pulse widths greater than 1 μs would likely be needed to excite thermographic phosphors in order to get the UV energies necessary to utilize CMOS-camera based data acquisition, this commercial LED driver was taken out of consideration for our phosphor thermometry experiments. The SNL driver was used in the rest of the work described in this paper.

Table 1 Ratio of the energy output from the 365-nm LED traces shown in Fig. 6 The energy output was calculated by integrating the voltage traces from the LED outputs at the varying pulse widths.

Input Signal Length	Ratio of Energy Output from LED (Sandia Driven/Commercially Driven)
1 μs	1.3096
2 μs	1.2743
3 μs	1.2872
4 μs	1.6919
5 μs	2.1235

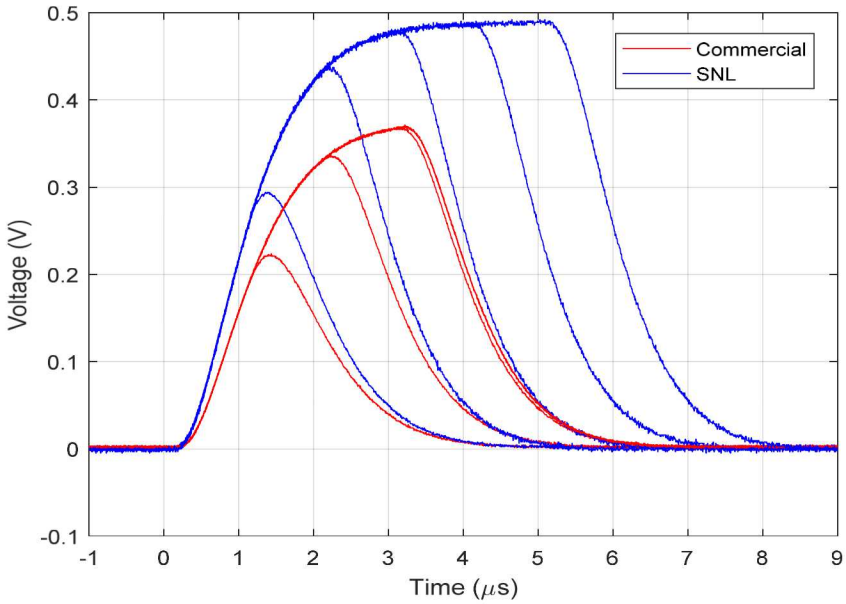

Fig. 6 Photodiode voltage acquired from 365-nm LEDs driven by commercial (red lines) and SNL (blue lines) drivers with 24V input power

Further characterization of the SNL driver was performed by varying the input voltage. Fig 7 shows the results of varying the input voltage of the SNL driver from 13 to 25 V, in 0.5 V increments. Each line represents the average of 4 runs at the same input voltage. A pulse width of 10 µs was used in this experiment. The peak photodiode voltage (approximately where the LED signal plateaus) appears to increase linearly with increasing input voltage. The rise and fall times also do not change dramatically with varying input voltage. These results show that, since the voltage signal from the photodiode correlates to LED power, the performance of this driver remains consistent between various input voltages.

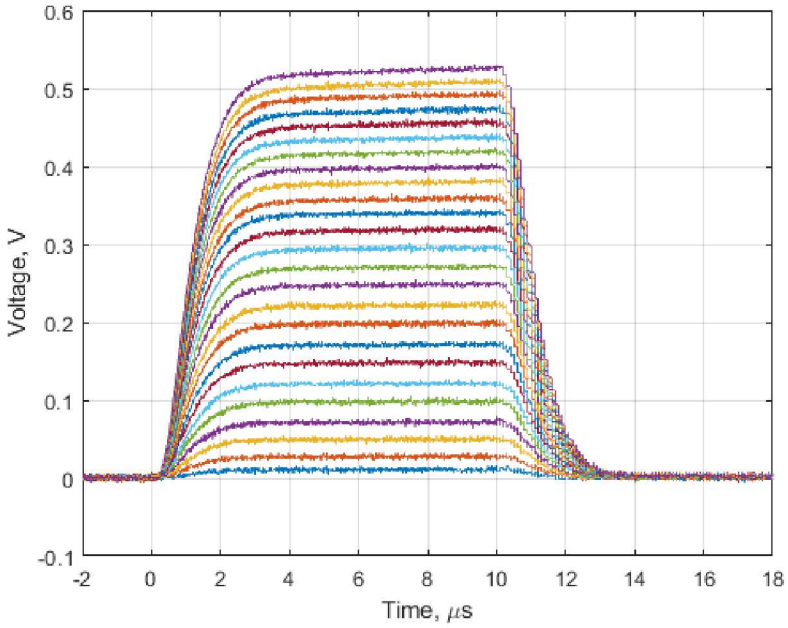

Fig. 7 The LED signals from the SNL driver with varying input voltage from 13 V (lowest blue line) to 25 V (highest purple line) with increments of 0.5 V.

B. Phosphor Furnace Calibration

Measurements were taken inside the calibration furnace from 100 to 600ºC in intervals of 50ºC. In order to test the impact of the LED pulse width on the measured time constants, five sets (corresponding to LED excitations of 1, 2, 3, 5, and 10 μs) of 100 time-series of images were taken at each temperature. The repetition rates were varied from 75 kHz (at the lowest temperatures) to 250 kHz at 600ºC in order to capture enough images to fit a time constant. For calibration, the signal was summed over the entire LED spot and then normalized to create time series like those shown in Fig. 7.

Backgrounds from the first 15 images in each time-series is subtracted off in order to limit the effect of graybody radiation from the furnace and then each time-series is individually fit in MATLAB with a non-linear least-square fit (Levenberg-Marquardt algorithm). The average results are plotted in Fig. 8 with the standard deviation as the error bars. For reference, the calibration curve for Mg_4FGeO_6:Mn from [13] is shown as a black line. As phosphors can vary from manufacturer and batch, calibrations are not expected to fall perfectly on top one another. As expected, little influence of LED pulse width can be seen in the time constants. A rational fit (numerator 4, denominator 5, Levenberg-Marquardt algorithm) was calculated in order to predict temperatures on the silicon carbide rod. The fit is shown with the blue dashed line. While the line fits the data well, there are areas of higher uncertainty. The first is between the temperatures of 400-500ºC. Because of the sparse data, an inflection point was fit here that is unlikely to exist based on published data. The second area of concern is at temperatures above 600ºC where our time constants decreases more quickly than what is seen in literature. Both of these problems can be fixed by taking addition future calibration measurements.

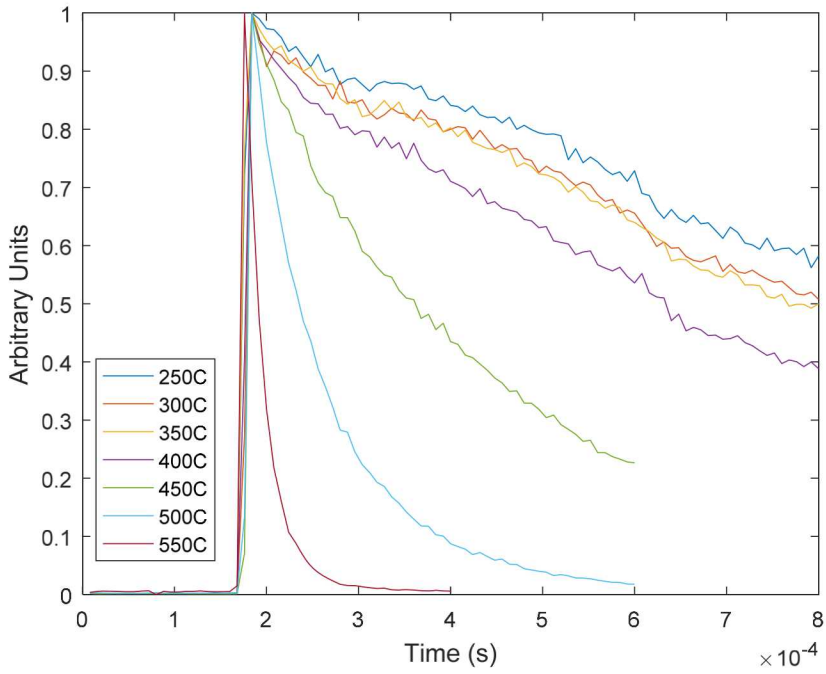

Fig. 8 Summed and normalized signals from a single time-series of images taken with an LED pulse width of 5 μs.

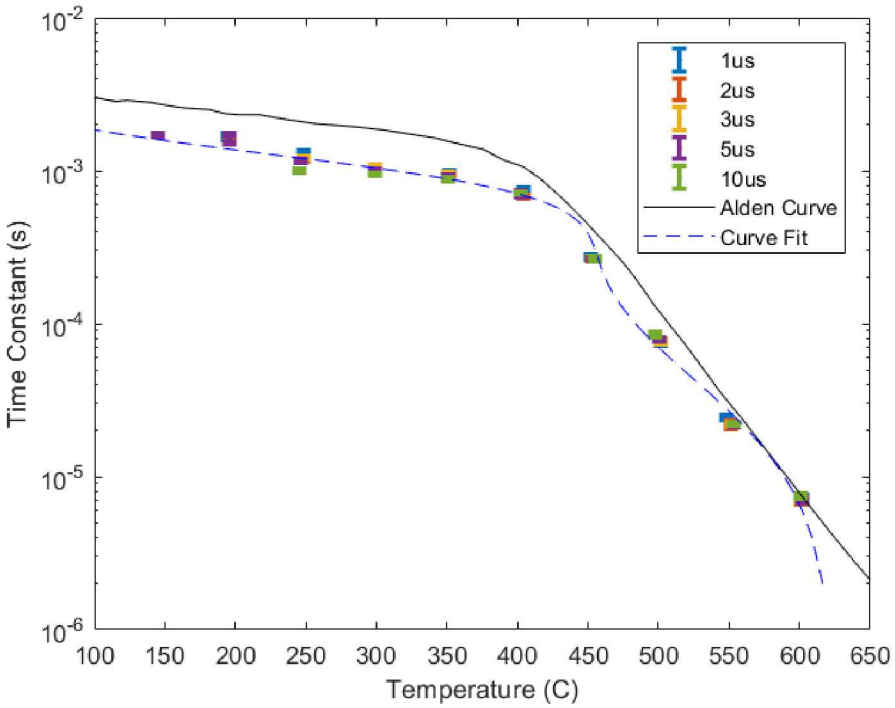

Fig. 9 Average time-decay constants for Mg_4FGeO_6:Mn measured in calibration oven with SNL-driven LED excitation of 1-10µs. Error bars represent one standard deviation of the 100 time-series taken at each temperature and pulse width.

C. Silicon Carbide Rod Temperatures

Power was cycled on and off to a silicon carbide rod-driven box heater in order to test the speed of the LED-excited thermographic phosphor temperature measurements. Images (Fig. 10, left) were processed in MATLAB, as above, with the signal binned 5x5 superpixels pre-fitting for their time-decay constant. The time-decay vs temperature curve fit shown in Fig. 9 was used to calculate a temperature corresponding to individual superpixels (Fig. 10, right). The averages and standard deviations, shown as error bars, can be seen in Fig. 11. The data acquisition rate of 250kHz was chosen in order to fully resolve the time-decay constants near 600ºC, however due to hardware limitations, this restricted time-series length to 350 images or ~1.3 milliseconds of active data collection after background images. Since the rule of thumb for good time-series fits is 4x the time constant, lower temperature data could not be fully resolved.

Of the two main areas of concern related to the curve fit discussed in Section IV.B., only the effects of the inflection point between 400-500ºC can be seen in the results shown in Fig. 11. As the power applied to the rod heaters was constant, the heating rate should have stayed constant as well. On the cooling side, the power was off, so no plateau in the cooling should have been seen around 450ºC. This error will likely be corrected by an increase in calibration data points as discussed above. The sharp drop in time-constants above 600ºC on the calibration curve was not an issue as none of the measured time decays in the heater experiment were faster those measured during calibration (7*10-6 s).

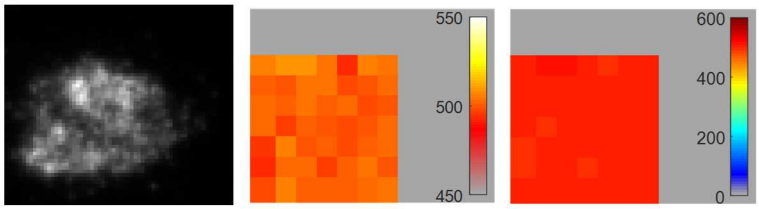

Fig. 10 Sample image (left) of phosphor spot on silicon carbide rod heater and its corresponding superpixel temperature map after processing (right). The temperature scale is 0-600ºC. Note that though the phosphor spot is not uniform, the processed temperatures are not affected.

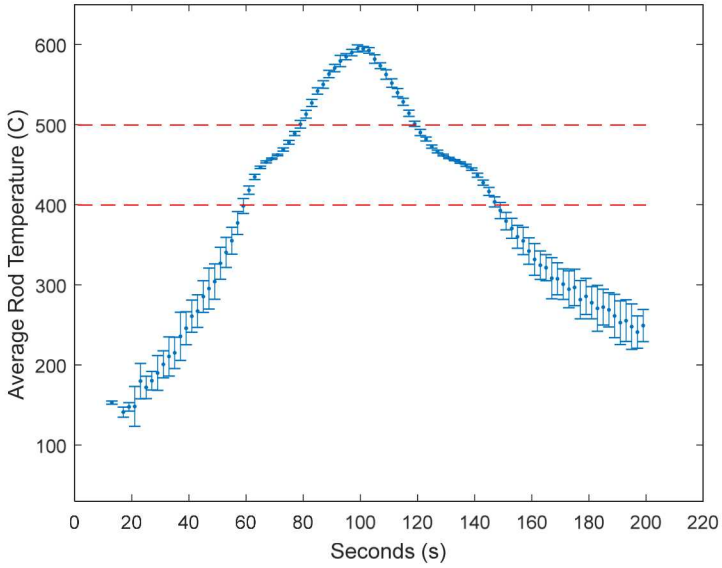

Fig. 11 Average measured temperature on the silicon carbide rod heater as power was applied and removed. Error bars are one standard deviation of the superpixel values.

V. Conclusion

The SNL-driven LED exhibits higher energy output than the commercially driven LED, making the Sandia driver preferable for replacing lasers for phosphor excitation. Additionally, the SNL driver's lack of pulse-limiting circuitry allows the LEDs to be overdriven resulting in more energy. Measurements in the calibration oven show only a small effect due to the pulse-width (up to 10µs) on temperature measurements using the Mg_4FGeO_6:Mn time-decay method.

Using the temperature-time constant fit calculated from the calibration measurements, silicon carbide rod temperatures were measured using an intensified CMOS camera at 250 kHz as power was cycled on and off. Temperatures above 400°C were resolved, but lower temperatures were difficult to fit due to recording-length limits on the intensifier. For future measurements, a lower repetition rate should be considered.

Acknowledgments

Sandia National Laboratories is a multimission laboratory managed and operated by National Technology & Engineering Solutions of Sandia, LLC, a wholly owned subsidiary of Honeywell International, Inc., for the U.S. Department of Energy's National Nuclear Security Administration under contract DE-NA0003525.

References

[1] Aldén, M., Omrane, A., Richter, M., and Särner, G., "Thermographic phosphors for thermometry: A survey of combustion applications," *Progress in Energy and Combustion Science*, vol. 37, 2011, pp. 422–461.

[2] Omrane, A., Wang, Y., Göransson, U., Holmstedt, G., and Aldén, M., "Intumescent coating surface temperature measurement in a cone calorimeter using laser-induced phosphorescence," *Fire Safety Journal*, vol. 42, 2007, pp. 68–74.

[3] Omrane, A., Ossler, F., Aldén, M., Svenson, J., and Pettersson, J. B. C., "Surface temperature of decomposing construction materials studied by laser-induced phosphorescence," *Fire and Materials*, vol. 29, 2004, pp. 39–51.

[4] Omrane, A., Ossler, F., Alden, M., Gtoransson, U., and Holmstedt, G., "Surface Temperature Measurement of Flame Spread Using Thermographic Phosphors," *Fire Safety Science*, vol. 7, 2003, pp. 141–152.

[5] Bartholmai, M., Schriever, R., and Schartel, B., “Influence of external heat flux and coating thickness on the thermal insulation properties of two different intumescent coatings using cone calorimeter and numerical analysis,” *Fire and Materials*, vol. 27, 2003, pp. 151–162.
[6] Blasi, C. D., and Branca, C., “Mathematical model for the nonsteady decomposition of intumescent coatings,” *AIChE Journal*, vol. 47, 2001, pp. 2359–2370.
[7] Yen, W. M., Shionoya, S., and Yamamoto, H., Phosphor handbook, Boca Raton: CRC Press, 2007.
[8] Nada, F. A., Knappe, C., Xu, X., Ritcher, M., and Alden, M., “On the automation of thermographic phosphor calibration,” *Institution of Engineering and Technology*, 2014.
[9] Brübach, J., Kissel, T., Frotscher, M., Euler, M., Albert, B., and Dreizler, A., “A survey of phosphors novel for thermography,” Journal of Luminescence, vol. 131, 2011, pp. 559–564.
[10] Feist, J., Heyes, A., Choy, K., and Su, B., “Phosphor thermometry for high temperature gas turbine applications,” ICIASF 99. 18th International Congress on Instrumentation in Aerospace Simulation Facilities. Record (Cat. No.99CH37025).
[11] Feist, J. P., Heyes, A. L., and Seefeldt, S., “Thermographic Phosphors for Gas Turbines: Instrumentation Development and Measurement Uncertainties,” 11th Int. Symp. Appl. Laser Tech. to Fluid Mech, 2002.
[12] Feist, J. P., Heyes, A. L., and Seefelt, S., “Thermographic phosphor thermometry for film cooling studies in gas turbine combustors,” Proceedings of the Institution of Mechanical Engineers, Part A: Journal of Power and Energy, vol. 217, 2003, pp. 193–200.
[13] Khalid, A. H., and Kontis, K., “Development of phosphor thermometry systems for use in development gas turbine engines,” thesis, 2011.
[14] Husberg, T., Gjirja, S., Denbratt, I., Omrane, A., Aldén, M., and Engström, J., “Piston Temperature Measurement by Use of Thermographic Phosphors and Thermocouples in a Heavy-Duty Diesel Engine Run Under Partly Premixed Conditions,” SAE Technical Paper Series, Nov. 2005.
[15] Allison, S. W., Beshears, D. L., Cates, M. R., Paranthaman, M., and Gilles, G. T., “LED-induced fluorescence diagnostics for turbine and combustion engine thermometry,” Optical Diagnostics for Fluids, Solids, and Combustion, 2001.
[16] Hradil, J., Davis, C., Mongey, K., Mcdonagh, C., and Maccraith, B. D., “Temperature-corrected pressure-sensitive paint measurements using a single camera and a dual-lifetime approach,” *Measurement Science and Technology*, vol. 13, Mar. 2002, pp. 1552–1557.
[17] Allison, S. W., Cates, M. R., and Gillies, G. T., “Excitation of thermographic phosphors using a blue light emitting diode: Spectral characteristics and instrumentation applications,” Review of Scientific Instruments, vol. 73, 2002, pp. 1832–1834.
[18] Atakan, B., Eckert, C., and Pflitsch, C., “Light emitting diode excitation of Cr3 :Al2O3as thermographic phosphor: experiments and measurement strategy,” Measurement Science and Technology, vol. 20, Oct. 2009, p. 075304.
[19] Westlye, F. R., Penney, K., Ivarsson, A., Pickett, L. M., Manin, J., and Skeen, S. A., “Diffuse back-illumination setup for high temporally resolved extinction imaging,” *Chinese Optics Letters* Available: https://www.osapublishing.org/ao/abstract.cfm?uri=ao-56-17-5028.
[20] “US9603210B1 - High speed, high current pulsed driver circuit,” *Google Patents* Available: https://patents.google.com/patent/US9603210B1/en.
[21] Kemeny, G., and Haake, C. H., “Activator Center in Magnesium Fluorogermanate Phosphors,” *The Journal of Chemical Physics*, vol. 33, 1960, pp. 783–789.
[22] Shao, Q., Lin, H., Hu, J., Dong, Y., and Jiang, J., “Temperature-dependent photoluminescence properties of deep-red emitting Mn4 -activated magnesium fluorogermanate phosphors,” *Journal of Alloys and Compounds* , vol. 552, 2013, pp. 370–375.
[23] Brübach, J., Zetterberg, J., Omrane, A., Li, Z., Aldén, M., and Dreizler, A., “Determination of surface normal temperature gradients using thermographic phosphors and filtered Rayleigh scattering,” *Applied Physics B*, vol. 84, 2006, pp. 537–541.
[24] Beshears, D., Capps, G., Simmons, C., and Schwenterly, S., “Laser-induced fluorescence of phosphors for remote cryogenic theromometry,” Jan. 1990.
[25] Brübach, J., Feist, J. P., and Dreizler, A., “Characterization of manganese-activated magnesium fluorogermanate with regards to thermographic phosphor thermometry,” *Measurement Science and Technology*, vol. 19, 2008, p. 025602.
[26] Goss, L. P., and Post, M. E., “Surface Thermometry of Energetic Materials by Laser-Induced Fluorescence.,” Jan. 1988.